Article

Electrochemical Oxidation of NADH at Nitrogen-Doped Carbon Nanotube Electrodes

Jacob Michael Goran, Carlos Alberto Favela, and Keith J. Stevenson

Anal. Chem., **Just Accepted Manuscript** • DOI: 10.1021/ac401784b • Publication Date (Web): 31 Aug 2013

Electrochemical Oxidation of NADH at Nitrogen-Doped Carbon Nanotube Electrodes

Jacob M. Goran[†], *Carlos A. Favela*[†], *Keith J. Stevenson*[†*]

[†]Department of Chemistry and Biochemistry, Center for Electrochemistry, Center for Nano- and Molecular Science and Technology, The University of Texas at Austin,

1 University Station, A5300, Austin, Texas 78712

*Stevenson@cm.utexas.edu

KEYWORDS

Electrocatalytic oxidation. Nicotinamide adenine dinucleotide. NADH. Carbon Nanotube. CNT. Nitrogen-doped carbon nanotube. N-CNT. Electrode Fouling. Glucose Dehydrogenase. NADH degradation. Glucose.

ABSTRACT

Nitrogen-doped carbon nanotubes (N-CNTs) substantially lower the overpotential necessary for NADH oxidation compared to nondoped CNTs or traditional carbon electrodes such as glassy carbon (GC). We observe a 370 mV shift in the E_p from GC to CNTs, and

another 170 mV shift from CNTs to 7.4 atom % N-CNTs in a sodium phosphate buffer solution (*p*H 7.0) with 2.0 mM NADH (scan rate 10 mV/s). The sensitivity of 7.4 atom % N-CNTs to NADH was measured at 0.30 ± 0.04 A M^{-1} cm^{-2}, with a limit of detection at 1.1 ± 0.3 μM, and a linear range of 70 ± 10 μM poised at a low potential of - 0.32 V (vs. Hg/Hg_2SO_4). NADH fouling, known to occur to the electrode surface during NADH oxidation, was investigated by measuring both the change in $E_{p,}$ and the resulting loss of electrode sensitivity. NADH degradation, known to occur in phosphate buffer, was characterized by absorbance at 340 nm and correlated with the loss of NADH electroactivity. N-CNTs are further demonstrated to be an effective platform for dehydrogenase based biosensing by allowing glucose dehydrogenase to spontaneously adsorb onto the N-CNT surface, and measuring the resulting electrode's sensitivity to glucose. The glucose biosensor had a sensitivity of 0.032 ± 0.003 A M^{-1} cm^{-2}, a limit of detection at 6 ± 1 μM, and a linear range of 440 ± 50 μM.

INTRODUCTION

Dihydronicotinamide adenine dinucleotide (NADH) is a cofactor for hundreds of dehydrogenase enzymes[1] commonly used for the design of electrochemical biosensors[1–4] and biofuel cells[5–7]. In order to continue the advance of dehydrogenase based biosensors and biofuel cells, there is a clear need to develop electrodes that can efficiently oxidize NADH to NAD^+, the necessary form of NADH that allows turnover of the enzymatic substrate. Oxidation of NADH at conventional electrode surfaces generally requires a large overpotential, which in-turn introduces a high background current and unwanted side reactions from electroactive interferents. This large overpotential also lowers the overall power density of a NADH-based

biofuel cell. In order to mitigate these deleterious effects, redox-active mediators are often introduced to lower the overpotential while efficiently shuttling electrons between NADH and the electrode surface.[1,2,8,9] Although effective in specified systems, redox mediators add another level of difficulty to the transport of electrons, and often must be immobilized or confined to ensure consistent results. An ideal electrode would inherently lower the oxidation overpotential, without additional mediation, referred to as an electrocatalyst. Although the differences between an electrocatalyst and a mediator are often not well defined, here we refer to mediators as any molecule that is not inherently part of the electrode material, and aids in the transfer of electrons from NADH to the electrode material. This includes covalently bound mediators found in chemically modified electrodes, physically adsorbed mediators, immobilized mediators (such as mediators within a hydrogel or polymer matrix), freely diffusing mediators, or even surface functionalities (which can be considered both mediators or inherently part of the electrode material) which were created on the electrode material post synthesis. Carbon nanotubes (CNTs), a unique carbon allotrope, were shown to exhibit electrocatalytic characteristics by dramatically lowering the NADH oxidation potential in comparison to glassy carbon by Wang and co-workers.[10–12] Carbon electrodes such as glassy carbon (GC) or highly ordered pyrolytic graphite (HOPG) are favored for bioanalytical applications since biomolecules such as enzymes have a higher tendency to denature at traditional noble metal electrode surfaces. The unique form of carbon found in CNTs significantly lowered the activation energy necessary to oxidize NADH, while also displaying higher resistance to surface fouling, known to occur during NADH oxidation.[13] Since that seminal discovery, a number of other studies related to the use of CNTs as an advanced electrode material for NADH oxidation have been performed. These include ordered CNTs[14], the use of dispersing agents such as hyaluronic acid[15], chitosan[16], mediators

including Meldola's blue[17], Variamine blue[18], TCBQ[19], toluidine blue,[20] toluidine blue O/chitosan matrix[21], poly(toluidine blue O)[22], poly(methylene green)/ carboxylated CNT composite[23], SWCNT "Bucky Paper"/poly(methylene green)[24], azure C/chitosan[25], azine/hydrogel[26], CNT/PDDA-poly(azure B) composite[27], CNT/DHB/nafion hybrid films[28], polyluminol/CNTs[29], 1,10-phenanthroline-5,6-dione[30], silica-azure C nanoparticles/CNTs/chitosan film[31], conducting polymers such as Poly-(3-methylthiophene)[32], PEDOP/MWCNT-Pd nanoparticles[33], PANI/PABS/SWCNTs,[34] dopamine/PEI/CNT composite[35], PDDA/PSS-[MWCNTs-NH_3^+-graphene-COO^-]$_5$,[36] carbodiimde coupled MWCNTs[37], and oxidative pretreatment of CNTs by microwave treatment in nitric acid[38]. In the vein of ideal NADH electrodes, heteroatom-doped CNTs have been shown to decrease the NADH oxidation potential without additional mediation. Boron-doped CNTs (B-CNTs), a p-type dopant in carbon, significantly enhanced the oxidation of NADH compared to nondoped CNTs.[39] Nitrogen-doped CNTs (N-CNTs), a n-type dopant in carbon, are cited as being both more biocompatible[40] and better electrocatalysts for important biomolecules such as H_2O_2.[41–43] Herein, we present an electrochemical investigation of NADH oxidation at N-CNTs, showing how incorporated nitrogen can further lower the overpotential and increase the sensitivity of CNTs to NADH as compared to glassy carbon (GC), edge plane pyrolytic graphite (EPPG), or nondoped CNTs. CNTs and N-CNTs were investigated without the use of binders, solubilizing/dispersing agents, or oxidative acid pretreatment as these have been shown to affect electrochemical performance.[38,44,45] The natural degradation of NADH in phosphate buffer and the effects of electrode fouling are also investigated, since degradation and electrode fouling are often difficult to distinguish between and must be taken into account for accurate analytical measurements. The use of N-CNTs as a platform for dehydrogenase-based biosensing are

demonstrated by allowing glucose dehydrogenase to spontaneously adsorb onto N-CNTs, subsequently creating a sensitive glucose biosensor.

EXPERIMENTAL

Enzyme and Chemicals

β-Nicotinamide adenine dinucleotide disodium salt hydrate, β-nicotinamide adenine dinucleotide dipotassium salt, α-D-glucose, *m*-xylene (anhydrous), and glucose dehydrogenase (from *Pseudomonas sp.,* E.C. 1.1.1.47, lyophilized powder ≥ 200 U/mg) were obtained from Sigma-Aldrich. Sodium phosphate monobasic (monohydrate), sodium phosphate dibasic (anhydrous), pyridine, and sodium hydroxide were purchased from Fisher. Bis(cyclopentadienyl)iron (ferrocene) was obtained from Alfa Aesar.

CNT/N-CNT Synthesis

CNTs and N-CNTs were synthesized by a chemical vapor deposition (CVD) process using ferrocene as a nucleation catalyst for CNT/N-CNT growth. A ferrocene solution of 20 mg mL^{-1} was prepared using *m*-xylene (CNTs) or pyridine (N-CNTs) and then pumped into a quartz tube at 0.1 mL min^{-1} through a glass syringe (Hamilton 8132) by an automated syringe pump (New Era Pump Systems NE-1000). The quartz tube was laid across two identical tube furnaces (Carbolite model HST 12/35/200/2416CG) which were set at different temperatures. The first furnace (where the ferrocene solution is injected into the quartz tube) was set at a temperature to ensure the solvent entered into the gas phase (150 °C for *m*-xylene and 130 °C for pyridine). Argon gas was used to direct the vaporized precursor along the quartz tube into the second

furnace, which was set at a temperature to initiate CNT/N-CNT growth along the inner diameter of the tube wall (700 °C for *m*-xylene and 800 °C for pyridine). Ammonia gas was introduced during N-CNT synthesis to increase the incorporated nitrogen content above the level set by the pyridine precursor (4.0 atom % N-CNTs). Incorporated nitrogen as a function of the ammonia flow rate was characterized in a prior report.[46] A total gas flow rate of 575 sccm was maintained during synthesis including H_2 gas for nondoped CNTs or NH_3 for N-CNTs above 4.0 atom % N-CNTs.

Electrochemistry and Electrode Preparation

Cyclic voltammograms (CVs) and chronoamperograms are plotted with a negative anodic current (pointing down) and a positive cathodic current (pointing up). Pine rotating disk electrodes (RDE, 5 mm diameter, AFE2M050) were polished using a 0.05 μm alumina slurry on a microfiber (Buehler) cloth, sonicated in nanopure (18 MΩ cm) water, and then rinsed with absolute ethanol. A mass normalized 24 μg of CNT/N-CNTs were drop cast on polished RDEs from a 2 mg mL^{-1} solution of N-CNTs, or a 0.4 mg mL^{-1} solution of CNTs in absolute ethanol, and allowed to air dry. CNT/N-CNT solutions were sonicated for 2 hours prior to use, to ensure a homogenous solution. Once dried, the CNT/N-CNT electrodes were wet with a mixture of ethanol and 0.10 M sodium phosphate buffer (SPB) at a *p*H of 7.0. CNT/N-CNT electrodes were cycled between (0 and -1.2 V vs Hg/Hg_2SO_4) in order to passivate residual electroactive iron remaining from synthesis.[47]. Electrochemical measurements were carried out with a Hg/Hg_2SO_4 reference electrode (CH Instruments, +0.64 V vs SHE; +0.44 V vs Ag/AgCl; +0.40 V vs SCE) and a coiled Au counter electrode using an Autolab PGSTAT30 potentiostat (GPES software version 4.9). NADH concentrations were calculated by mass, assuming one water molecule was

associated with the disodium salt hydrate, and that the NADH (either disodium salt hydrate or anhydrous dipotassium salt) was 100% pure. Error associated from the purity assumption would only cause the electrochemical sensitivity measurements to be underestimated.

RESULTS AND DISCUSSION

Electrocatalytic Oxidation of NADH at CNT/N-CNT Electrodes

Figure 1 displays cyclic voltammograms (CVs) of glassy carbon (GC), edge plane pyrolytic graphite (EPPG), nondoped CNT, 4.0 atom % N-CNT, and 7.4 atom % N-CNT electrodes in 0.10 M sodium phosphate buffer (SPB) at a *p*H of 7.0 in the presence of 2.0 mM NADH. The oxidation peak potential of NADH (E_p) dramatically decreases from traditional carbon electrodes such as GC and EPPG to the CNT electrodes, with an additional decrease when nitrogen is introduced into the CNT lattice. It is often cited that the increased edge plane character of CNT imparts electrocatalytic activity for NADH oxidation.[48,49]

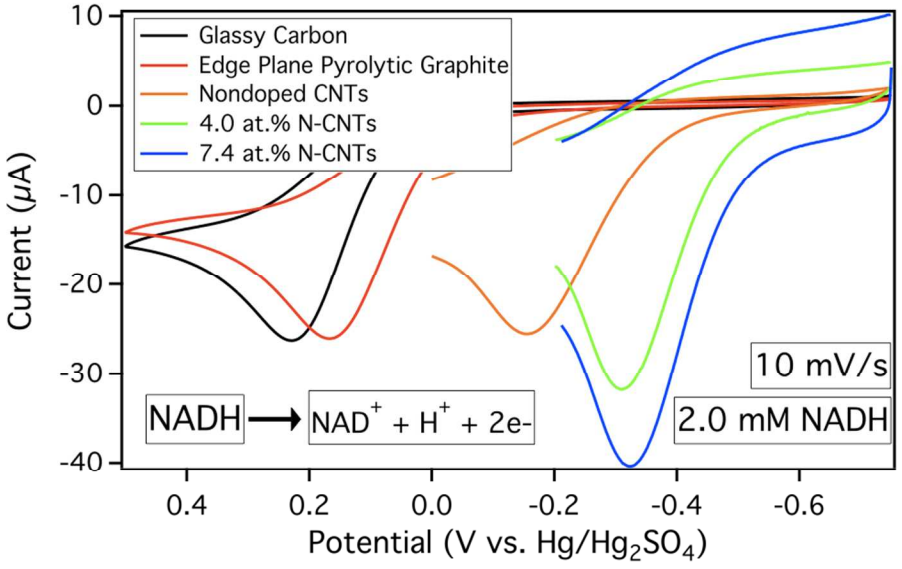

Figure 1. Oxidation of 2.0 mM NADH at glassy carbon, edge plane pyrolytic graphite, nondoped CNT, 4.0 atom % N-CNT, and 7.4 atom % N-CNT electrodes at a scan rate of 10 mV/s in 0.10 M SPB (*p*H 7.0).

Incorporation of nitrogen into CNTs has been shown to increase the edge plane character of CNTs,[46,50,51] thereby increasing their electrocatalytic activity towards NADH oxidation. Nitrogen-doping, however, is distinctly different than a simple increase in the edge plane density of an all carbon lattice, elegantly visualized as a single nitrogen dopant in nitrogen-doped graphene.[52] For N-CNTs, both the type and density of reactive surface sites (which now may involve nitrogen) and the electronic properties of the electrode material (such as the density of states and charge carrier density) are altered due to the n-type dopant, both of which affect the overall electrode kinetics.[51,53,54] Furthermore, the sidewalls of CNTs have been clearly shown to be active sites for electron transfer, thereby suggesting that edge plane character is not solely indicative of observed electrochemical behavior.[55] We aim to investigate a simple preparation of these carbon surfaces, alumina polish for GC/EPPG electrode surfaces and drop casting of CNT/N-CNT electrodes, to accurately determine a base level of NADH reactivity, without additional surface treatments, binders, dispersing agents, or NADH mediators. The results in Figure 1 suggests that N-CNTs both increase the oxidation current, probably due to the increased surface area of N-CNTs[51], and decrease the potential at which NADH oxidation occurs. Table 1 presents the peak potential (E_p) for NADH oxidation at each of the electrodes shown in Figure 1. The Supporting Information displays each oxidation peak (from Figure 1) with its respective background (Figure S-1). Nondoped CNTs lower the oxidation potential by 370 mV from GC, while N-CNTs further lower the potential by 170 mV compared to nondoped CNTs. There is only a modest decrease in the E_p (20 mV) between 4.0 atom % N-CNTs and 7.4 atom % N-

CNTs. Overall, there is a 540 mV decrease in the E_p from GC to our 7.4 atom % N-CNT electrodes. It should be pointed out that the standard deviation for E_p is smaller at N-CNTs compared to GC, EPPG, or nondoped CNTs.

Table 1. Oxidation peak potentials (E_p) of 2mM NADH in 0.1 M SPB (*p*H 7) at 10 mV/s

Type	E_p (V vs. Hg/Hg_2SO_4)	# of Trials	ΔE_p from GC (mV)
GC	+ 0.22 ± 0.05	51	0
EPPG	+ 0.17 ± 0.04	31	50
Nondoped CNTs	- 0.15 ± 0.04	48	370
4.0 atom % N-CNTs	- 0.30 ± 0.02	24	520
7.4 atom % N-CNTs	- 0.32 ± 0.01	26	540

The E_p is often used as a figure of merit for NADH electrocatalysts; however, E_p is highly dependent on experimental conditions. Early work done by Moiroux and Elving[56–58] and Blaedel and Jenkins[59] indicated that variables such as scan rate, concentration of NADH, supporting electrolyte, and pretreatment as well as prior conditioning of the electrode surface play an important role in the observed potential of NADH oxidation. Analysis of NADH oxidation is further confounded by electrode fouling, NADH degradation, and other factors such as uncompensated resistance, making E_p an inconsistent metric for comparison between electrocatalysts. In general, a less positive E_p is observed at slower scan rates and lower concentrations of NADH. Figure S-2 in the Supporting Information displays CVs of 4.0 atom % N-CNTs in the presence of 0.5, 1.0, 2.0, 4.0, and 8.0 mM NADH at both 50 and 100 mV/s. Table S-3 (Supporting Information) identifies the shift in E_p as a function of NADH concentration from Figure S-2. The oxidation peak shifts positive concurrent with both increasing concentrations of NADH and scan rate. Figure S-4 and Table S-5 in the Supporting Information show the shift in E_p as a function of scan rate from 10 mV/s to 200 mV/s in a constant concentration of 2.0 mM

NADH (also at a 4.0 atom % N-CNT electrode). The observed E_p shifts under these measurements conditions, which are relatively standard conditions, can vary up to 200 - 300 mV. With such a wide range of E_p values based on standard operating conditions, it is clear why E_p becomes an inconsistent metric between NADH electrocatalysts. Quantitative assessment of NADH oxidation can also be characterized by measuring the sensitivity of an electrode to NADH, poised at a constant potential, as discussed below in the NADH sensitivity section. In order to attempt a comparison of NADH oxidation electrode materials, the Supporting Information displays a table (Table S-15) of CNT based NADH oxidation electrodes found in the literature.

It has been reported in the literature that nondoped CNTs will sometimes display two NADH oxidation peaks.[10,48] This phenomenon has been ascribed to NADH oxidation at the background electrode, on which the CNTs are applied.[48] This additional E_p, however, is often between that reported for CNTs or the E_p of NADH at the background electrode. Although not consistently, we observe two NADH oxidation peaks at CNTs in addition to a wave associated with the background electrode (Supporting Information Figure S-6). We also observe two oxidation peaks if CNTs are drop cast on GC or Au background electrodes (Supporting Information Figure S-7).

NADH Sensitivity

The sensitivity of each electrode material to NADH was determined by rotating disk amperometry, where the concentration of NADH was increased while the electrode was poised at a constant potential (i.e. the steady-state current at each concentration was recorded relative to the background). The potential at which the electrode was poised plays a major role in determining the sensitivity to NADH. The Supporting Information (Figure S-8 and Table S-9)

presents the sensitivity of a 7.4 atom % N-CNT electrode to 5 μM aliquots of NADH as a function of potential. The results point out that although the sensitivity of the linear range stays fairly constant, the linear range is clearly extended at higher potentials. A better way to characterize the increased performance at higher potentials (since the constantly changing linear ranges have similar sensitivities) is to compare the electrode sensitivity at a constant NADH concentration (in this case 50 μM, or the average response of the first 10 aliquots). Table 2 displays the sensitivity (based on the linear range) of each type of electrode material to NADH, along with the linear range, limit of detection, sensitivity to 50 μM NADH, and poised potential, which was chosen to be the E_p from Figure 1. It appears that the GC and EPPG electrodes have the highest sensitivity to NADH, however, the poised potential is significantly higher than the CNT/N-CNT electrodes. If the 7.4 atom % N-CNTs are poised at the same potential as GC, the sensitivity is slightly higher than that of GC, but more importantly, the linear range is significantly extended. Furthermore, if the GC electrode is poised at the potential for CNTs or either type of N-CNTs, the observed oxidation current is insignificant, as seen in the Supporting Information (Figure S-10), which displays representative chronoamperograms for each electrode material from Table 2, and the coordinating background (GC) current for comparison.

Table 2. Sensitivity to NADH measured by rotating disk amperometry

Type	Sensitivity ($A\ M^{-1}\ cm^{-2}$)	Limit of Linear Range (μM)	Limit of Detection (μM)	Poised Potential (V vs. Hg/Hg_2SO_4)
GC	0.37 ± 0.03	410 ± 80	0.4 ± 0.2	0.22
EPPG	0.35 ± 0.04	270 ± 100	0.5 ± 0.2	0.17
Nondoped CNTs	0.21 ± 0.06	40 ± 20	0.6 ± 0.2	- 0.15
4.0 atom % N-CNTs	0.27 ± 0.04	40 ± 10	0.8 ± 0.2	- 0.30
7.4 atom % N-CNTs	0.30 ± 0.04	70 ± 10	1.1 ± 0.3	- 0.32
7.4 atom % N-CNTs	0.38 ± 0.02	> 600	1.0 ± 0.3	0.22

Electrochemical Fouling

It is well know that oxidation of NADH fouls the electroactive surface of the working electrode.[1,2,13] Fouling is most commonly ascribed to the adsorption of the oxidation product NAD^+ (a self-inhibitory oxidation reaction)[48,60] and the formation of dimers, created by radical intermediates.[61] The initial electron transfer from NADH creates a cation radical which subsequently deprotonates forming a neutral radical which can dimerize. There are claims that CNTs mitigate fouling when compared to GC.[10] Given that the incorporated nitrogen in N-CNTs causes significant differences in their physical properties as compared to nondoped CNTs (such as a more positive surface charge at *p*H 7.0)[46,50,51], we investigated electrode fouling from NADH oxidation on N-CNT electrodes compared to nondoped CNT, EPPG, and GC electrodes. Figure 2 presents CVs of a 7.4 atom % N-CNT electrode cycled in 2.0 mM NADH for 10 cycles at 10 mV/s, and extensively fouled by cycling at 500 mV/s for 1000 cycles (checked periodically at 10 mV/s). Figures S-11 and S-12 in the Supporting information present identical CVs for all 5 types of electrode materials used in this study. As one would expect, fouling is visualized in the

CVs as an increasing overpotential (peak shifts more positive) and a decrease in the peak current as the surface sites become inhibited.

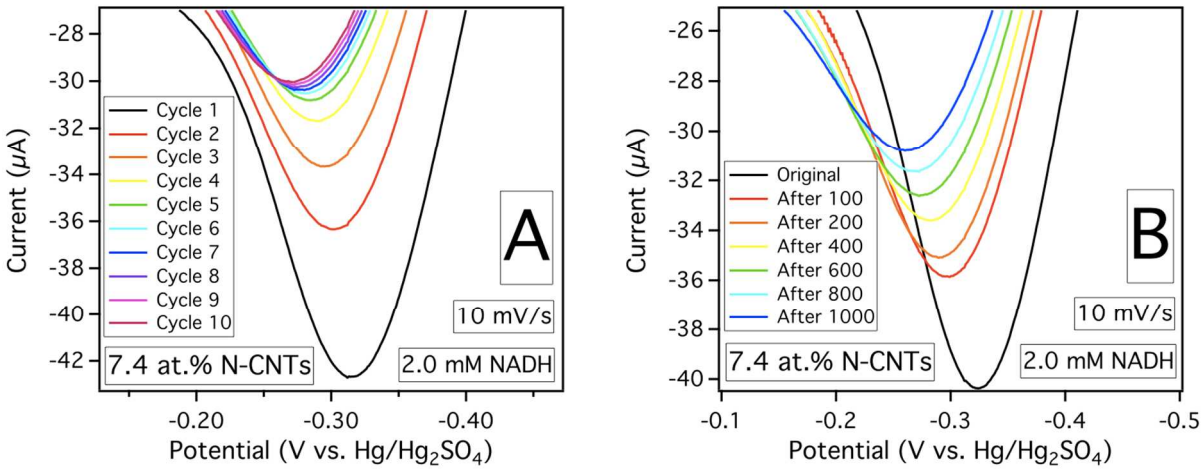

Figure 2. CVs of a 7.4 at.% N-CNT electrode cycled in 2.0 mM NADH for (A) 10 cycles at 10 mV/s or (B) 1000 cycles at 500 mV/s (measured at 10 mV/s, 0.10 M SPB, *p*H 7.0).

Interestingly, nondoped CNTs will often display an increasing peak current, although the overpotential is still increased (Figure S-11C and S-12C). Fouling is electroactivated and not spontaneous, as freshly made N-CNT electrodes cycled once in 2.0 mM NADH at 10 mV/s, allowed to sit for the timeframe of eight cycles and subsequently cycled once more, display E_p shifts identical to the second cycle of continuously cycled electrodes. Table 3 presents the E_p shift for each type of electrode material for both the 10 cycles at 10 mV/s and the 1000 cycles at 500 mV/s (which were measured periodically at 10 mV/s). The shift after 10 cycles seems to suggest that the traditional carbon electrodes are more resistant to fouling. After 1000 cycles, the shift is fairly random across the 5 electrode types, making any assessment of fouling based on the E_p shift difficult; however, the sensitivity of each type of electrode to NADH was also measured after the extensive fouling. Sensitivity analysis indicates that the CNT/N-CNT

electrodes are more resistant to fouling as compared to the traditional carbon electrodes. N-CNTs do not show any significant advantage to nondoped CNTs with respect to NADH fouling.

Table 3. E_p shift for NADH oxidation in 2.0 mM NADH and sensitivity to NADH after extensive fouling (0.10 M SPB *p*H 7.0)

Type	10 cycles at 10 mV/s (mV)	1000 cycles at 500 mV/s (mV)	Sensitivity Remaining (after 1000 cycles)
GC	40 ± 10	80 ± 30	21 %
EPPG	30 ± 10	70 ± 40	37 %
Nondoped CNTs	40 ± 10	40 ± 10	81 %
4.0 atom % N-CNTs	70 ± 10	100 ± 40	70 %
7.4 atom % N-CNTs	60 ± 10	70 ± 10	76 %

NADH Degradation

An important aspect of measuring NADH oxidation is the degradation of NADH in solution, especially phosphate buffer.[23,62] NADH displays an absorbance at 340 nm due to the pyridine ring of nicotinamide. This absorbance can be monitored over time as NADH degrades in solution displayed in the equation below as the percent degradation (eq 1):

$$\% \text{ Degradation } = 100 - ((A_t/A_{(t=0)}) \times 100) \quad (1)$$

Where A_t is the absorbance at time t, t is the time elapsed since NADH was placed in solution, and $A_{(t=0)}$ is the initial absorbance (at t = 0). This procedure provides a reasonable estimate of NADH degradation; however, since the decrease in absorbance at 340 nm is indicative of the disruption of the nicotinamide pyridine ring, the electroactivity should be correlated. As previously mentioned, electrode fouling confounds these measurements, but pre-fouled electrodes can correlate degradation and electroactivity with minimal fouling interference. Figure S-13 in the Supporting Information shows chronoamperograms of a pre-fouled 7.4 atom

% N-CNT electrode where either fresh or degraded NADH is injected into solution. The fresh NADH, used both before and after the degraded NADH is injected, overlay quite well, allowing the sensitivity loss due to degradation to be accurately measured. NADH degradation as measured by UV-vis displayed a linear degradation rate of 2.2 ± 0.1% per hour, over eight hours of measurements. This value remained true after NADH was used immediately after purchase or continuously used over 3 months, being stored at - 20°C when not in use. Figure 3A displays the change in absorbance at 340 nm over eight hours. The degradation rate was non-linear over a longer timeframe, as this rate should have no absorbance after 45.5 hours. Figure 3B displays the normalized absorbance (normalized to the initial absorbance) as measured over 104 hours. The electroactivity scales reasonable well with the decrease in the absorbance, with the normalized electroactivity (normalized to a fresh NADH sample) generally being slightly higher than the normalized absorbance at any given timepoint. At approximately 50 hours, the UV-vis absorbance is 34 % of the initial absorbance while the electroactivity is 40% that of a fresh NADH solution. At approximately 100 hours the UV-vis absorbance is at 14 % while the electroactivity is at 17 %. The sensitivity loss of 7.4 atom % N-CNTs to NADH due to degradation in the linear regime (the first 8 hours) was found to decrease at 0.006 ± 0.001 A M^{-1} cm^{-2} hr^{-1}.

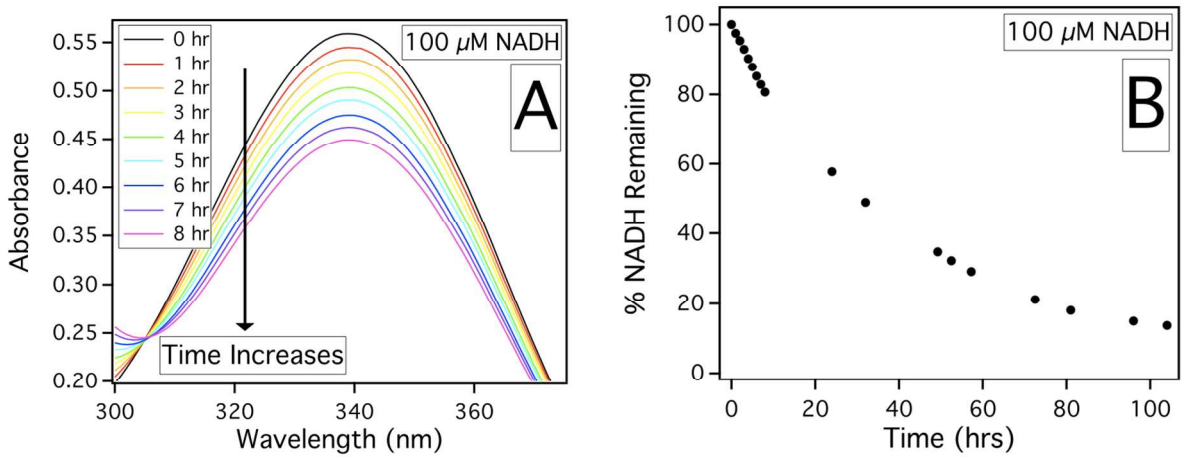

Figure 3. UV-Vis spectra displaying the decrease in the absorbance of the nicotinamide peak centered at 340 nm over 8 hours (A) or the normalized absorbance over 104 hours (B) in 0.10 M SPB (*p*H 7.0).

Demonstration of NADH Biosensing using Glucose Dehydrogenase

Dehydrogenase enzymes will convert NAD^+ to NADH in the presence of an appropriate substrate. Since N-CNTs can effectively detect NADH by oxidation at a low potential, N-CNTs were coupled with glucose dehydrogenase (GDH) to demonstrate their utility as a functional biosensing material. N-CNTs were previously shown to display spontaneous adsorption of biologically active enzyme[63], thus, we choose to allow GDH to adsorb onto the N-CNT surface from a 20 μM GDH solution (0.10 M SPB *p*H 7.0). Figure 4 presents the sensitivity of GDH loaded 7.4 atom % N-CNT electrodes to 50 μM injections of glucose as a function of adsorption time (Table S-14 in the Supporting Information displays the biosensing figures of merit for each adsorption timepoint). The sensitivity to glucose increases concurrently with adsorption time until 20 min, where the sensitivity begins to decrease with increased GDH loading. This

observation suggests that there is a balance between available surface sites where NADH oxidation occurs, and the surface coverage of GDH (which blocks reactive sites).

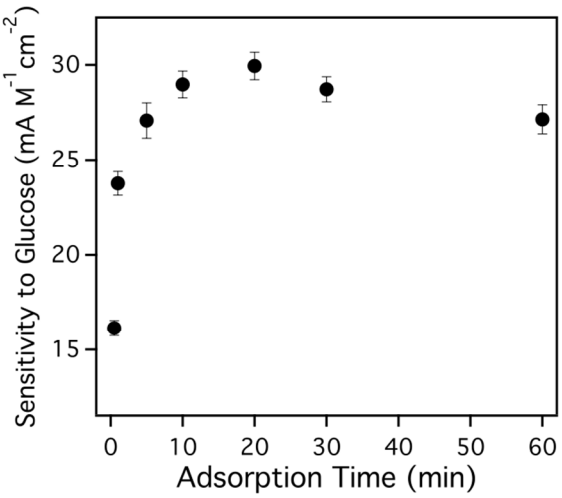

Figure 4. The sensitivity of a GDH loaded 7.4 atom % N-CNT electrode to glucose as a function of adsorption time in a 20 μM GDH solution (0.10 M SPB *p*H 7.0).

The glucose biosensor displayed a linear range up to 440 ± 50 μM, a limit of detection at 6 ± 1 μM, and a sensitivity of 0.032 ± 0.003 A M^{-1} cm^{-2} (based on the linear range) in a 0.10 M SPB solution with 2.0 mM NAD^+. Figure 5A presents a representative chronoamperogram of a 7.4 atom % N-CNT electrode with adsorbed GDH (20 min) as 50 μM glucose injections are introduced. Figure 5B displays the corresponding anodic current response (absolute value) as a function of glucose concentration.

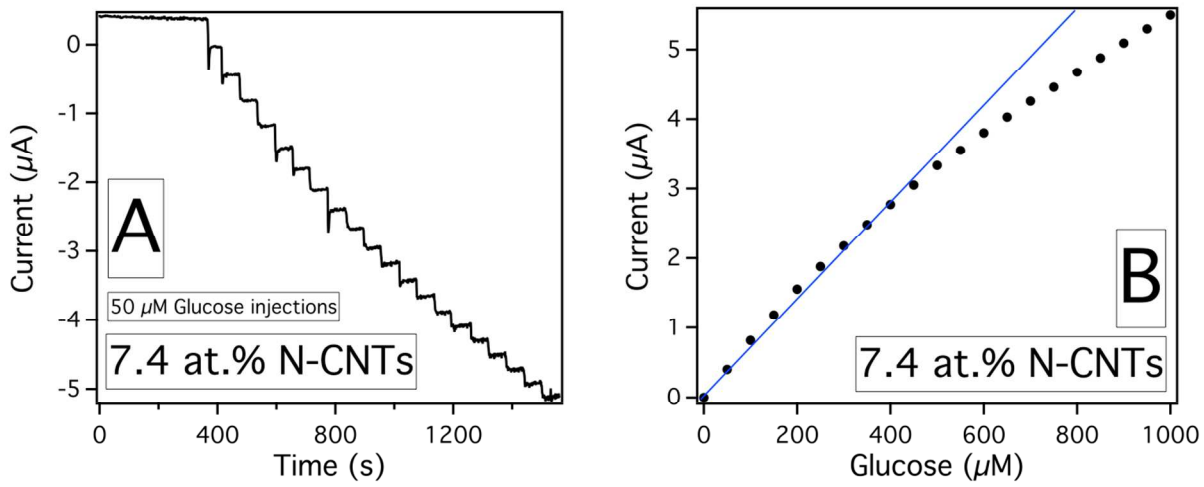

Figure 5. Chronoamperogram of a GDH loaded (20 min in a 20 μM GDH solution) 7.4 atom % N-CNT rotating disk electrode (1000 rpm) to 50 μM injections of glucose (A) and the corresponding anodic current response as a function of glucose concentration (B, line indicates linear range).

Compared to the sensitivity of 7.4 atom % N-CNTs to direct injections of NADH (Table 2), the sensitivity of the glucose biosensor to glucose is only 11%. Although the available surface sites for NADH oxidation are expected to decrease as GDH is adsorbed onto the surface, and the local formation of NADH is determined by the orientation of the adsorbed GDH, there appears to be room for improvement. Nonetheless, the N-CNT electrodes offer a simple platform to create a multitude of biosensors from the spontaneous adsorption of enzymes.

Enzyme kinetics were measured for the adsorbed GDH electrodes where at -0.32 V (vs. Hg/Hg_2SO_4) the glucose concentration was increased until saturation. The apparent Michaelis constant (K_M^{app}) and the maximum velocity (V_{max}) were determined from Lineweaver-Burk plots. Values of 2.9 ± 0.2 mM for K_M^{app} and 106 ± 6 pmol/s for V_{max} were obtained. Since the sensitivity of NADH is strongly dependent on potential, we issue a word of caution when

measuring enzyme kinetics. The strong potential dependency indicates that the electrooxidation of NADH is probably a kinetically limited reaction, since the enzymatic reaction should be spontaneous and independent of electrode potential. When enzyme kinetics were measured at 0.17 V, the same amount of glucose did not saturate the electrode, and the K_M^{app} and V_{max} were 9.9 mM and 398 pmol/s, respectively. Since these values are over 3 times that measured at -0.32 V (and well beyond the standard deviation at that potential) we can confidently assume that the measured kinetic parameters are arising from the electrochemical reaction, rather than the spontaneous enzymatic reaction.

CONCLUSION

N-CNTs were shown to be electrocatalytic towards the oxidation of NADH as compared to nondoped CNTs or traditional carbon electrodes. The sensitivity of 7.4 atom % N-CNTs to NADH (poised at a low applied potential of – 0.32 V vs. Hg/Hg_2SO_4) rivals that of the best CNT-based electrodes, even when mediators are included. Fouling of the electrode surface from NADH oxidation was characterized by E_p and the resulting electrode sensitivity loss. Although the shifting E_p made comparison between electrode types difficult, CNT/N-CNT electrodes displayed a higher resistance to fouling based upon the sensitivity loss after extensive fouling. The degradation of NADH in 0.10 M SPB was characterized by absorbance at 340 nm and correlated with the loss of NADH electroactivity. The enhanced electroactivity toward NADH and spontaneous adsorption of dehydrogenase enzyme provides a simple platform for dehydrogenase-based biosensing using N-CNTs, as demonstrated using glucose dehydrogenase as a model enzyme. Future studies will investigate the reaction kinetics of NADH oxidation at N-CNTs.

ASSOCIATED CONTENT

Supporting Information includes 10 figures and 5 tables as noted in the text. This material is available free of charge via the Internet at http://pubs.acs.org.

ACKNOWLEDGMENT

Financial support of this work was provided by the R.A. Welch Foundation (grant F-1529). CAF acknowledges support from NSF-REU program (grant CHE-1003947).

REFERENCES

(1) Lobo, M.; Miranda, A.; Tuñón, P. *Electroanalysis* **2005**, *9*, 191–202.
(2) Radoi, A.; Compagnone, D. *Bioelectrochem.* **2009**, *76*, 126–134.
(3) Wang, J. *Electroanalysis* **2005**, *17*, 7–14.
(4) Katakis, I.; Domínguez, E. *Microchim. Acta* **1997**, *32*, 11–32.
(5) Barton, S. C.; Gallaway, J.; Atanassov, P. *Chem. Rev.* **2004**, *104*, 4867–4886.
(6) Willner, I.; Yan, Y.-M.; Willner, B.; Tel-Vered, R. *Fuel Cells* **2009**, *9*, 7–24.
(7) Meredith, M. T.; Minteer, S. D. *Annu. Rev. Anal. Chem.* **2012**, *5*, 157–179.
(8) Gorton, L.; Domínguez, E. *Rev. Mol. Biotechnol.* **2002**, *82*, 371–392.
(9) Gründig, B.; Wittstock, G.; Rüdel, U.; Strehlitz, B. *J. Electroanal. Chem.* **1995**, *395*, 143–157.
(10) Musameh, M.; Wang, J.; Merkoci, A.; Lin, Y. *Electrochem. Commun.* **2002**, *4*, 743–746.
(11) Wang, J.; Musameh, M. *Anal. Chem.* **2003**, *75*, 2075–2079.
(12) Wang, J.; Deo, R. P.; Poulin, P.; Mangey, M. *J. Am. Chem. Soc.* **2003**, *125*, 14706–14707.
(13) Wang, J.; Angnes, L.; Martinez, T. *Bioelectrochem. Bioenerg.* **1992**, *29*, 215–221.
(14) Chen, J.; Bao, J.; Cai, C.; Lu, T. *Anal. Chim. Acta* **2004**, *516*, 29–34.
(15) Filip, J.; Sefčovičová, J.; Tomčík, P.; Gemeiner, P.; Tkac, J. *Talanta* **2011**, *84*, 355–361.
(16) Zhang, M.; Smith, A.; Gorski, W. *Anal. Chem.* **2004**, *76*, 5045–5050.
(17) Zhu, L.; Zhai, J.; Yang, R.; Tian, C.; Guo, L. *Biosens. Bioelectron.* **2007**, *22*, 2768–2773.
(18) Radoi, a.; Compagnone, D.; Valcarcel, M. a.; Placidi, P.; Materazzi, S.; Moscone, D.; Palleschi, G. *Electrochim. Acta* **2008**, *53*, 2161–2169.
(19) De Cássia Silva Luz, R.; Damos, F. S.; Tanaka, A. A.; Kubota, L. T.; Gushikem, Y. *Elelctrochim. Acta* **2008**, *53*, 4706–4714.
(20) Lawrence, N. S.; Wang, J. *Electrochem. Commun.* **2006**, *8*, 71–76.
(21) Zhang, M.; Gorski, W. *J. Am. Chem. Soc.* **2005**, *127*, 2058–2059.
(22) Zeng, J.; Wei, W.; Wu, L.; Liu, X.; Liu, K.; Li, Y. *J. Electroanal. Chem.* **2006**, *595*, 152–160.
(23) Li, H.; Wen, H.; Calabrese Barton, S. *Electroanalysis* **2012**, *24*, 398–406.
(24) Narváez Villarrubia, C. W.; Rincón, R. a; Radhakrishnan, V. K.; Davis, V.; Atanassov, P. *ACS Appl. Mater. Interfaces* **2011**, *3*, 2402–2409.
(25) Zhang, M.; Gorski, W. *Anal. Chem.* **2005**, *77*, 3960–3965.
(26) Meredith, M. T.; Giroud, F.; Minteer, S. D. *Elelctrochim. Acta* **2012**, *72*, 207–214.
(27) Gao, Q.; Sun, M.; Peng, P.; Qi, H.; Zhang, C. *Microchim. Acta* **2010**, *168*, 299–307.
(28) Raj, C. R.; Chakraborty, S. *Biosens. Bioelectron.* **2006**, *22*, 700–706.
(29) Lin, K. C.; Yin, C. Y.; Chen, S. M. *Analyst* **2012**, *137*, 1378–1383.
(30) Mao, X.; Wu, Y.; Xu, L.; Cao, X.; Cui, X.; Zhu, L. *Analyst* **2011**, *136*, 293–298.
(31) Karra, S.; Zhang, M.; Gorski, W. *Anal. Chem.* **2012**, *85*, 1208–1214.
(32) Agüí, L.; Peña-Farfal, C.; Yáñez-Sedeño, P.; Pingarrón, J. M. *Elelctrochim. Acta* **2007**, *52*, 7946–7952.
(33) You, J.-M.; Jeon, S. *Elelctrochim. Acta* **2011**, *56*, 10077–10082.

(34) Liu, J.; Tian, S.; Knoll, W. *Langmuir* **2005**, *21*, 5596–5599.
(35) Gasnier, A.; Pedano, M. L.; Gutierrez, F.; Labbé, P.; Rivas, G. A.; Rubianes, M. D. *Elelctrochim. Acta* **2012**, *71*, 73–81.
(36) Prasannakumar, S.; Manjunatha, R.; Nethravathi, C.; Suresh, G. S.; Rajamathi, M.; Venkatesha, T. V. *J. Solid State Electrochem.* **2012**, *16*, 3189–3199.
(37) Sun, Y.; Ren, Q.; Liu, X.; Zhao, S.; Qin, Y. *Biosens. Bioelectron.* **2013**, *39*, 289–295.
(38) Wooten, M.; Gorski, W. *Anal. Chem.* **2010**, *82*, 1299–1304.
(39) Deng, C.; Chen, J.; Chen, X.; Xiao, C.; Nie, Z.; Yao, S. *Electrochem. Commun.* **2008**, *10*, 907–909.
(40) Carrero-Sanchez, J. C.; Elías, a L.; Mancilla, R.; Arrellín, G.; Terrones, H.; Laclette, J. P.; Terrones, M. *Nano Lett.* **2006**, *6*, 1609–1616.
(41) Tang, Y.; Allen, B. L.; Kauffman, D. R.; Star, A. *J. Am. Chem. Soc.* **2009**, *131*, 13200–13201.
(42) Xu, X.; Jiang, S.; Hu, Z.; Liu, S. *ACS Nano* **2010**, *4*, 4292–4298.
(43) Goran, J. M.; Lyon, J. L.; Stevenson, K. J. *Anal. Chem.* **2011**, *83*, 8123–8129.
(44) Pelster, L. N.; Meredith, M. T.; Minteer, S. D. *Electroanalysis* **2012**, *24*, 1011–1018.
(45) Lawrence, N.; Deo, R.; Wang, J. *Electroanalysis* **2005**, *17*, 65–72.
(46) Maldonado, S.; Morin, S.; Stevenson, K. J. *Carbon* **2006**, *44*, 1429–1437.
(47) Lyon, J. L.; Stevenson, K. J. *Langmuir* **2007**, *23*, 11311–11318.
(48) Banks, C. E.; Compton, R. G. *Analyst* **2005**, *130*, 1232–1239.
(49) Moore, R. R.; Banks, C. E.; Compton, R. G. *Anal. Chem.* **2004**, *76*, 2677–82.
(50) Maldonado, S.; Morin, S.; Stevenson, K. J. *Analyst* **2006**, *131*, 262–267.
(51) Wiggins-Camacho, J. D.; Stevenson, K. J. *J. Phys. Chem. C* **2009**, *113*, 19082–19090.
(52) Zhao, L.; He, R.; Rim, K. T.; Schiros, T.; Kim, K. S.; Zhou, H.; Gutiérrez, C.; Chockalingam, S. P.; Arguello, C. J.; Pálová, L.; Nordlund, D.; Hybertsen, M. S.; Reichman, D. R.; Heinz, T. F.; Kim, P.; Pinczuk, A.; Flynn, G. W.; Pasupathy, A. N. *Science* **2011**, *333*, 999–1003.
(53) Cline, K.; McDermott, M.; McCreery, R. *J. Phys. Chem.* **1994**, *98*, 5314–5319.
(54) McCreery, R. L. *Chem. Rev.* **2008**, *108*, 2646–2687.
(55) Güell, A. G.; Ebejer, N.; Snowden, M. E.; McKelvey, K.; Macpherson, J. V; Unwin, P. R. *Proc. Natl. Acad. Sci.* **2012**, *109*, 11487–11492.
(56) Moiroux, J.; Elving, P. J. *Anal. Chem.* **1978**, *50*, 1056–1062.
(57) Moiroux, J.; Elving, P. J. *Anal. Chem.* **1979**, *51*, 346–350.
(58) Moiroux, J.; Elving, P. J. *J. Am. Chem. Soc.* **1980**, *1337*, 6533–6538.
(59) Blaedel, W.; Jenkins, R. *Anal. Chem.* **1975**, *47*, 1337–1343.
(60) Blankespoor, R.; Miller, L. *J. Electroanal. Chem.* **1984**, *171*, 231–241.
(61) Jaegfeldt, H. *Bioelectrochem. Bioenerg.* **1981**, *128*, 355–370.
(62) Rover, L. J.; Fernandes, J. C.; de Oliveira Neto, G.; Kubota, L. T.; Katekawa, E.; Serrano, S. H. *Anal. Biochem.* **1998**, *260*, 50–55.
(63) Goran, J. M.; Mantilla, S. M.; Stevenson, K. J. *Anal. Chem.* **2013**, *85*, 1571–1581.

FOR TOC ONLY: